PAPER

CrossMark
click for updates

Highly flexible all-solid-state cable-type supercapacitors based on Cu/reduced graphene oxide/manganese dioxide fibers†

Miaomiao Huang,[abc] Lu Wang,[abc] Shuangbao Chen,[abc] Liping Kang,[abc] Zhibin Lei,[abc] Feng Shi,[abc] Hua Xu[abc] and Zong-Huai Liu*[abc]

Highly flexible all-solid-state cable-type supercapacitors based on Cu/reduced graphene oxide/manganese dioxide fibers (Cu/RGO/MnO$_2$) were successfully assembled by closely placing two Cu/RGO/MnO$_2$ fibers in a parallel direction and using PVA–KOH gel electrolyte, in which the Cu/RGO/MnO$_2$ fiber electrode, possessing good flexibility, excellent electrochemical properties, and high electrical conductivity was prepared by heating a glass pipeline filled with a Cu wire and a graphene oxide homogenous suspension at 230 °C for 2.5 h. The Cu/reduced graphene fiber was then refluxed in KMnO$_4$ solution at 70 °C for 120 min. As well as being used as a current collector, the Cu wire also served as the matrix for depositing active materials and improving the fiber flexibility, causing a high-quality interfacial contact between the current collector and the active materials. The optimized all-solid-state Cu/RGO/MnO$_{2(6.0)}$ fiber supercapacitor showed a high specific capacitance of 140 mF cm^{-2} at a current density of 0.1 mA cm^{-2}, enhanced capacitance retention of 97% after 500 bending cycles with a big angle of 120°, and relatively good stability (88% of initial capacitance values after 5000 cycles). Moreover, aside from its excellent electrochemical performance, it could light a LED lamp when connected with a battery, indicating that the assembled Cu/RGO/MnO$_2$ fiber supercapacitor could be used not only as an energy storage device, but also an electrical conduction cable, which could have a significant impact on future energy storage applications.

1. Introduction

Recently, all solid-state supercapacitors integrating electrodes, solid electrolytes and separators into a single entity have attracted tremendous attention because of their low weight, good flexibility, high capacitance and safety.[1,2] They are also much more suitable for developing fiber supercapacitors with flexibility and good electrochemical properties.[3,4] To develop all-solid-state fiber supercapacitors with good flexibility and excellent capacitance, the design and preparation of the fiber electrodes with these same properties are very important. In general, carbon based fibers[5–7] are used as the flexible electrode material and the constructed carbon based fiber supercapacitors show a relatively low performance, although they also possess good flexibility and are lightweight.[8–10] Therefore,

the flexible electrode materials for all-solid-state fiber supercapacitors with a high capacitance and energy density still need to be designed and prepared.

It is well known that graphene has been widely explored as an electrode material for high-performance supercapacitors because of its high surface area, good electrical conductivity, and chemical stability.[11] Most importantly, graphene can be assembled into one-dimensional fibers with remarkable features including high strength, electrical and thermal conductivities, low weight and ease of functionalization.[12,13] These graphene fibers have prominent advantages over common carbon based fibers for application in fiber-based devices while maintaining the basic characteristics of graphene.[14,15] However, graphene fiber supercapacitors still show a relatively low capacitance due to the lack of structure optimization and inefficiency of the pseudocapacitance, therefore limiting their applications as high performance fiber supercapacitors.[16] In order to improve their capacitive performance, some pseudocapacitive materials such as MnO$_2$, RuO$_2$, Fe$_2$O$_3$, etc. are incorporated into graphene fibers.[17–20] Among them, MnO$_2$–graphene fiber supercapacitors have been designed and prepared due to their outstanding characteristics such as high theoretical specific capacitance ($\sim$1400 F g^{-1}), natural abundance, and environmental friendliness,[21] for example

^{a}Key Laboratory of Applied Surface and Colloid Chemistry, Shaanxi Normal University, Ministry of Education, Xi'an, 710119, P. R. China. E-mail: zhliu@snnu.edu.cn; Fax: +86-29-8153-0702; Tel: +86-29-8153-0706

^{b}Shaanxi Key Laboratory for Advanced Energy Devices, Xi'an, 710119, P. R. China

^{c}School of Materials Science and Engineering, Shaanxi Normal University, Xi'an, 710119, P. R. China

PPy@MnO$_2$@rGO deposited conductive yarns,[22] GF–MnO$_2$ composite fibers,[23] graphene fiber-based asymmetric microsupercapacitors,[24] MnO$_2$-modified hierarchical graphene fiber,[25] CuO@AuPd@MnO$_2$ core–shell NWs,[26] hierarchical MnO$_2$ nanowire/graphene hybrid fibers,[27] C/MnO$_2$ core–shell fiber,[28] δ-MnO$_2$/holey graphene hybrid fiber,[29] etc. However, incorporating MnO$_2$ causes the flexibility and electrical conductivity of the prepared fiber electrodes to decrease because of the poor electrical conductivity and rigidity of these transition metal oxides.[30] Therefore, it is still a challenge to further improve the electrical conductivity and flexibility of the transition metal oxide–graphene fiber electrodes in order to construct all-solid-state fiber supercapacitors also with these properties.

Not long ago, the Thomas group developed a coaxial cable concept, in which both the inner and outer conductors share the same geometric axis and both the electrical conduction and energy storage properties can be integrated into the same cable.[26] This will revolutionize energy storage applications, and makes combining two different functional devices into one device possible. It is well known that one of the major roles of current collectors in supercapacitors is to effectively collect/transport charge carriers (e.g., electrons) from/to the active materials during the charge and discharge processes. Thus, a high-quality interfacial contact between the current collector and the active material is highly desirable to reduce the contact resistance and lead to high power and rate capabilities.[31] Based on the coaxial cable concept and aiming to further improve the electrical conductivity and flexibility of the transition metal oxide–graphene fiber electrodes for constructing all-solid-state fiber supercapacitors with good flexibility and excellent capacitance, the Cu/RGO/MnO$_2$ fiber electrode with good flexibility, excellent electrochemical properties, and high electrical conductivity was prepared. The synthesis consisted of heating a glass pipeline filled with a Cu wire (150 μm in diameter) and a graphene oxide homogenous suspension at 230 °C for 2.5 h, followed by refluxing the Cu/RGO fiber in KMnO$_4$ solution at 70 °C for 120 min. By then closely placing two Cu/RGO/MnO$_2$ fibers in a parallel orientation and using PVA–KOH gel electrolyte, the highly flexible, all-solid-state cable-type supercapacitors based on the Cu/RGO/MnO$_2$ fiber electrodes were finally assembled. They not only exhibited a high specific capacitance of 140 mF cm^{-2} at a current density of 0.1 mA cm^{-2}, an enhanced capacitance retention of 97% after 500 bending cycles with a big angle of 120°, and a relatively good stability (88% of initial capacitance values after 5000 cycles), but also could light an LED lamp after it is fully charged or serve as a conductive cable connecting the lamp lit with a battery, suggesting that the assembled Cu/RGO/MnO$_2$ fiber supercapacitor could be used as an energy storage device as well as an electrical conduction cable. This has high impact on the future energy storage applications.

2. Experimental

2.1 Materials preparation

All chemicals used in this experiment were of analytical grade and used without further treatment. Graphene oxide (GO) was purchased from Nanjing XFNANO Material Technology Company Limited. 120 mg of GO was dispersed into ultrapure water (10 mL) and treated by ultrasonication in a water bath for 4 h, and a homogeneous GO suspension (12 mg mL^{-1}) was obtained.

The Cu/reduced graphene oxide (Cu/RGO) fibers were prepared by an improved one-step dimensionally-confined hydrothermal strategy,[32] in which the Cu wire was selected as the fiber-formed center and current collector. In a typical process, the Cu wire with both a length of 7 cm and a diameter of 150 μm was firstly cleaned in acetone for 1 min and then was washed with distilled water. It was then placed into a glass pipeline with a 0.5 mm inner diameter, and the GO homogenous suspension (1 mL, 12 mg mL^{-1}) was injected into the glass pipeline using a syringe and its nozzle was sealed with an alcohol burner. The glass pipeline served as a hydrothermal reactor and was baked in an oven at 230 °C for 2.5 h. The reduced graphene oxide nanosheets (RGO) were coated on the surface of the Cu wire, and Cu/RGO fibers matching the pipe geometry were obtained. The preformed Cu/RGO fiber was taken by a nipper from the pipeline, which had a diameter of about 160 μm in its wet state and was placed on glass slides for drying in air. The dried Cu/RGO fiber almost maintained its length but its diameter reduced to about 152 μm due to water loss. The as-prepared Cu/RGO fiber showed good flexibility, and could be bent to any angle by hands.

The Cu/RGO fibers (10 mg) were then soaked in a 6.0 mM KMnO$_4$ solution (50 mL) in a 150 mL flask. The reaction system was stirred for 5 min and then refluxed at 70 °C for 120 min. The nanostructured δ-MnO$_2$ was successfully deposited on the surface of the Cu/RGO fibers via in situ reaction between carbon and KMnO$_4$, and thus the Cu/RGO/MnO$_{2(6.0)}$ fiber electrode was finally prepared after it was washed with deionized water and dried in a vacuum oven. By changing the concentrations of the KMnO$_4$ solution, Cu/RGO/MnO$_{2(M)}$ fiber electrodes with different MnO$_2$ coating amounts were obtained by a similar process, in which M was the concentration of KMnO$_4$ solution.

2.2 Material characterization

The morphology of the Cu/RGO/MnO$_2$ fiber electrodes was observed on a TM-3000 scanning electron microscope (SEM) and an SU8020 field-emission scanning electron microscope (FESEM). X-ray diffraction (XRD) patterns were obtained on a D/Max-3c instrument operating at 40 kV and 20 mA, using Cu Kα radiation ($\lambda = 1.5406$ Å). Raman spectra were measured and collected using a Renishaw inVia Raman microscope with an excitation wavelength of 532 nm. A Q600 thermoanalyzer system was used to analyze the content of carbon upon heating from room temperature to 800 °C in air. X-ray photoelectron spectroscopy (XPS) was performed with AXIS ULTRA (Kratos Analytical Ltd.) using Kα radiation (1486.6 eV) as an excitation source. To ensure the accuracy of the data measured, all of the binding energies were calibrated relative to the C 1s peak (284.6 eV) from the hydrocarbon adsorbed on the surface of Cu/RGO/MnO$_2$ fiber electrodes.

2.3 Electrochemical measurement

The flexible symmetric all-solid-state cable-type fiber super-capacitor based on the $Cu/RGO/MnO_2$ fiber electrode was assembled using the $Cu/RGO/MnO_2$ fiber as both the positive and negative electrodes. In order to avoid the risk of a short circuit caused by uneven coating from polyvinyl alcohol (PVA–KOH) electrolyte, the $Cu/RGO/MnO_2$ fiber was firstly coated with PVA gel and then immersed in KOH solution. The PVA gel was prepared by adding 3.0 g of PVA into 30 mL deionized water, followed by steadily heating at 85 °C and vigorously stirring until the mixture became clear, and then it was naturally cooled to room temperature. Two $Cu/RGO/MnO_2$ fibers were closely placed in a parallel orientation, and immersed into the PVA gel for 3 h and then dried at room temperature until the coated PVA gel had solidified. After repeating this two times, the two $Cu/RGO/MnO_2$ fibers were successfully assembled together by the viscosity of the PVA gel. The $Cu/RGO/MnO_2$ fibers coated with PVA gel were then immersed into 6 M KOH solution (30 mL) for 12 h, and a flexible symmetrical all-solid-state fiber super-capacitor based on the $Cu/RGO/MnO_2$ fiber electrode was successfully assembled after it was packaged with PTFE film. Cyclic voltammetry (CV) and galvanostatic charge–discharge tests were carried out with a CHI660E electrochemical work-station (CH Instruments Inc. China) in a two-electrode system in the PVA–KOH gel electrolyte. The capacitance C of the supercapacitor was calculated by using the equation: $C = I/(dV/dt)$, where I and dV/dt were the discharge current and the slope of the discharge curve, respectively. The area specific capaci-tance C_A was derived from the equation: $C_A = C/A$, where $A = \pi \times L \times D$ (L is the device length and D is the diameter of the fiber electrode).

3. Results and discussion

The formation process schematic of the all-solid-state cable-type fiber supercapacitor based on the $Cu/RGO/MnO_2$ fiber electrode is presented in Fig. 1. In order to increase the inter-facial contact between the current collector and the active material and to reduce the contact resistance, the Cu wire has been selected as both the current collector and the fiber-formed center in the present work. At first, the Cu wire, with both a length of 7 cm and a diameter of 150 μm, is placed into a glass pipeline with a 0.5 mm inner diameter, and GO homogenous suspension is injected into the glass pipeline by using a syringe. The glass pipeline is then baked in an oven at 230 °C for 2.5 h,

the reduced graphene oxide nanosheets (RGO) are coated on the surface of the Cu wire, and the Cu/RGO fibers matching the pipe geometry are obtained. Secondly, when the Cu/RGO fiber is soaked in $KMnO_4$ solution and refluxed at 70 °C for 120 min, δ-MnO_2 with a regular inter-connected structure is deposited on the surface of the Cu/RGO fiber via in situ reaction between carbon and $KMnO_4$, and the $Cu/RGO/MnO_2$ fiber electrode is prepared by washing it with deionized water and drying in a vacuum oven. Thirdly, the flexible symmetric all-solid-state cable-type fiber supercapacitor based on the $Cu/RGO/MnO_2$ fiber electrode is assembled by using the $Cu/RGO/MnO_2$ fiber as both positive and negative electrodes. Two $Cu/RGO/MnO_2$ fibers are closely placed in a parallel orientation, and are immersed into the PVA gel and then immersed in KOH solution in order to avoid the risk of a short circuit caused by uneven coating from the PVA–KOH electrolyte.

Because the coated amount of MnO_2 on the surface of the Cu/RGO fiber affects the capacitance of the assembled symmetrical supercapacitor due to its pseudocapacitance characteristic, the coated amount is firstly investigated by changing the concentration of the $KMnO_4$ solution, and the FESEM images and XRD patterns of the obtained Cu/RGO/MnO_2 fibers are studied. It can be seen that the morphologies of the $Cu/RGO/MnO_2$ fibers have obvious differences (Fig. S1†). When the amount of coated MnO_2 is small or large, the nano-structured δ-MnO_2 cannot be homogeneously distributed throughout the surface of the Cu/RGO fiber and the regular inter-connected MnO_2 arrays cannot be formed. On the other hand, MnO_2 can be homogeneously distributed throughout the surface of the Cu/RGO fiber and the regular inter-connected MnO_2 arrays are formed for the $Cu/RGO/MnO_{2(6.0)}$ fiber elec-trode when the Cu/RGO fiber is soaked in 6.0 mM $KMnO_4$ solution and refluxed at 70 °C for 120 min. In order to better understand the effect of the coated MnO_2 amount on the microstructure of the Cu/RGO fiber, the XRD patterns of the Cu/RGO/MnO_2 fibers obtained from different MnO_2 coating amounts are given in Fig. S2.† It can be seen that the XRD pattern of the Cu/RGO fiber exhibits a broad peak at 25.3°, corresponding to the (002) plane of the stacked reduced gra-phene sheets.[33] The XRD patterns of the $Cu/RGO/MnO_2$ fibers obtained from different amounts of coated MnO_2 indicate that a weak typical diffraction peak at 12.3° corresponding to the (001) plane of δ-MnO_2 can be indexed except the diffraction peak around 25.3° for the Cu/RGO fiber,[34] suggesting that δ-MnO_2 with a layered structure is formed on the surface of the Cu/RGO fiber. Moreover, the peak intensity hardly changes with
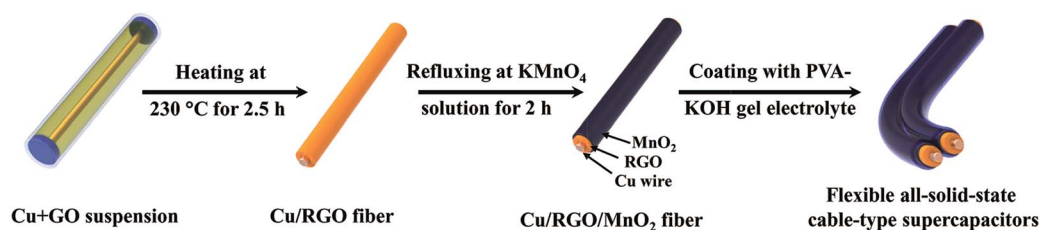

Fig. 1 Schematic preparation representation of the all-solid-state cable-type supercapacitor based on the $Cu/RGO/MnO_2$ fiber electrode.

the coated amount of MnO_2, indicating the weak crystallinity of the formed δ-MnO_2.

The birnessite-type structure of the formed δ-MnO_2 on the surface of the Cu/RGO fiber is further confirmed by the Raman spectra (Fig. S3,† above). Except from the D band (about 1350 cm^{-1}) and G band (1590 cm^{-1}) associated with the reduced graphene oxide,[35] one feature peak at 645 cm^{-1} is observed for the Cu/RGO/MnO_2 fibers due to the existence of δ-MnO_2. The experimental data is in good agreement with the major vibrational features of δ-MnO_2 reported previously,[36] supporting that MnO_2 with a birnessite-type layered structure is formed. In addition, the amount of δ-MnO_2 coated on the surface of the Cu/RGO fibers, calculated from their TG-DTA curves (Fig. S3,† below), and by scraping them off the Cu wire, are around 16%, 52% and 36% for the Cu/RGO/$MnO_{2(4.0)}$, Cu/RGO/$MnO_{2(6.0)}$, and Cu/RGO/$MnO_{2(7.0)}$ fiber electrodes, respectively. Among these fiber electrodes, the Cu/RGO/$MnO_{2(6.0)}$ fiber electrode shows the largest amount of coated MnO_2. It also possesses the regular inter-connected MnO_2 arrays on the surface of the Cu/RGO fiber and it could potentially show good electrochemical properties when is assembled into a symmetrical supercapacitor.

Therefore, the flexible symmetrical all-solid-state cable-type fiber supercapacitors based on Cu/RGO/MnO_2 fiber electrodes are assembled, and their cyclic voltammetry (CV), charge–discharge curves and electrochemical impedance spectroscopy (EIS) are tested in a two-electrode system in PVA–KOH gel electrolyte, and the experimental results are shown in Fig. 2. Compared with the CV curve area of the symmetrical Cu/RGO at 50 mV s^{-1} in a range of 0.0 to 0.8 V $vs.$ SCE, the closed CV curve area for the symmetrical Cu/RGO/MnO_2 fiber supercapacitors becomes larger in the company of increased amounts of coated MnO_2, suggesting that the capacitance of the symmetrical Cu/RGO/MnO_2 fiber supercapacitor can be improved by increasing the loading amount of the nanostructured MnO_2 (Fig. 2, left). Moreover, the symmetrical Cu/RGO/$MnO_{2(6.0)}$ fiber supercapacitor exhibits the largest CV area, indicating that it has the largest specific capacitance of all the symmetrical Cu/RGO/MnO_2 fiber supercapacitors. The higher specific capacitance may be ascribed to two aspects. One is that the amount of δ-MnO_2 coated on the surface of the Cu/RGO fiber is the largest in

the Cu/RGO/MnO_2 fiber electrodes, increasing pseudocapacitance and its full utilization. Another is that the Cu wire as the current collector not only reduces the contact resistance, but also improves the electrical conductivity of the fiber electrode. In addition, all CV curves show a typically rectangular shape and no obvious faradaic current, suggesting that these symmetrical Cu/RGO/MnO_2 fiber supercapacitors possess an ideal EDLC behavior at the electrode/electrolyte interface.[37] Also the same trend can be found by comparing the GCD curves of the symmetrical Cu/RGO/MnO_2 fiber supercapacitors at a current density of 0.3 mA cm^{-2} (Fig. 2, middle). All of the charging curves are symmetrical with their corresponding discharge counterparts and show good linear voltage–time profiles, indicating good capacitive behavior of the symmetrical Cu/RGO/MnO_2 fiber supercapacitors. In comparison with the specific capacitance of the symmetrical Cu/RGO fiber supercapacitor (20 mF cm^{-2}) and the other two symmetrical Cu/RGO/MnO_2 fiber supercapacitors (37–70 mF cm^{-2}), the symmetrical Cu/RGO/$MnO_{2(6.0)}$ fiber supercapacitor shows the largest area specific capacitance of 80 mF cm^{-2}.

In order to further investigate the charge transfer at the interface of the electrolyte-hybrid electrode, the Nyquist plots of the symmetrical Cu/RGO and Cu/RGO/MnO_2 fiber supercapacitors over a frequency range of 0.01 Hz to 100 kHz are tested, and the experimental results are shown in Fig. 2, right. It can be seen that their Nyquist plots are composed of a straight line at the lower frequency region and a semicircle at the higher frequency region. For the symmetrical Cu/RGO fiber supercapacitor, its Nyquist plot shows a smaller semicircle than those of the symmetrical Cu/RGO/MnO_2 fiber supercapacitors, suggesting that the symmetrical Cu/RGO fiber supercapacitor shows low charge transfer resistance.[38] Moreover, although all symmetrical Cu/RGO/MnO_2 fiber supercapacitors show a similar vertical line, the symmetrical Cu/RGO/$MnO_{2(6.0)}$ fiber supercapacitor shows the most vertical line, suggesting that the conductive links between MnO_2 and RGO provide an enhanced electrical conductivity or easily accessible ion path for electrolyte ions.[39] Although the manganese oxide electrode shows low electron conductivity because of its semiconductor characteristic,[40] the electrical conductivity of the symmetrical Cu/RGO/$MnO_{2(6.0)}$ fiber supercapacitor is improved, suggesting that Cu
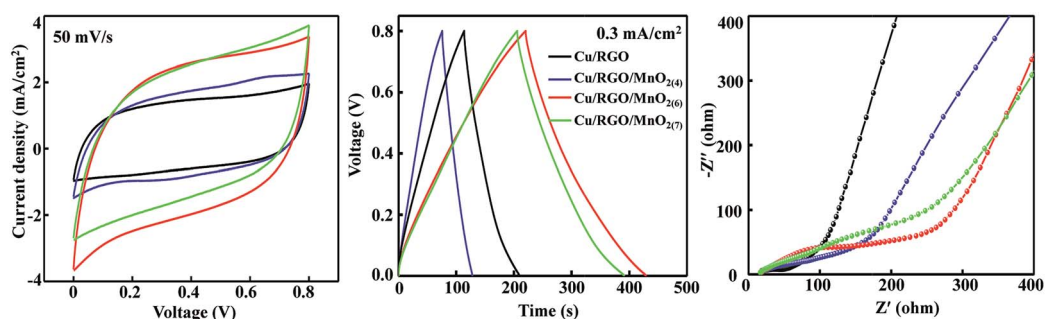

Fig. 2 Electrochemical characterization of the all-solid-state cable-type supercapacitor based on Cu/RGO/MnO_2 fibers coated with different amounts of MnO_2: CV curves at a scan rate of 50 mV s^{-1} (left), galvanostatic charge/discharge curves at a current density of 0.3 mA cm^{-2} (middle), and Nyquist plots over the frequency range of 100 kHz to 0.1 Hz (right).

wire as the current collector is favorable for improving the electrical conductivity of the Cu/RGO/MnO$_{2(6.0)}$ fiber electrode. These experimental results suggest that the symmetrical Cu/RGO/MnO$_{2(6.0)}$ fiber supercapacitor shows good capacitive performance. Therefore, the flexible all-solid-state symmetrical Cu/RGO/MnO$_{2(6.0)}$ fiber supercapacitor is further investigated.

An SEM image of the flexible all-solid-state symmetrical Cu/RGO/MnO$_{2(6.0)}$ fiber supercapacitor is shown in Fig. 3a. It shows a rough outer surface with a diameter of around 150 μm. The micro-morphology is further investigated by field-emission scanning electron microscopy (FE-SEM), and the MnO$_2$ nanostructure with inter-connected arrays uniformly grows on the Cu/RGO fiber (Fig. 3b). Moreover, the energy dispersive spectroscopy (EDS) mapping for the fibre axial direction also shows the existence of C, O, Mn and Cu elements, suggesting that the nanostructured MnO$_2$ is homogeneously distributed throughout the Cu/RGO fiber (Fig. 3c). Additionally, the manganese oxidation state in Cu/RGO/MnO$_{2(6.0)}$ fiber is very important when it is used as an electrode material for a supercapacitor, and is confirmed by XPS analysis; the experimental result is showed in Fig. 4. Two peaks at 642.7 eV and 653.9 eV are observed and can be attributed to the binding energies of Mn 2p$_{3/2}$ and Mn 2p$_{1/2}$ with a spin energy separation of 11.8 eV

(above). The binding energy values agree well with those of the reported MnO$_2$, indicating that a large number of Mn(IV) ions exist in the Cu/RGO/MnO$_2$ fiber electrode.[41] In addition, its mean manganese oxidation number is also calculated by using the energy separation between the two peaks of the Mn 3s core level spectrum (below). The peak energy separation value is 4.9 eV, and the average manganese oxidation number in the Cu/RGO/MnO$_{2(6.0)}$ fiber electrode is 3.7 on the basis of an approximately linear relationship between the splitting width and the Mn oxidation state is reported by the Brousse and Park group.[42,43]

By using the Cu/RGO/MnO$_{2(6.0)}$ fiber as the assembling unit, the flexible all-solid-state symmetrical Cu/RGO/MnO$_{2(6.0)}$ fiber supercapacitors are assembled, and their mechanical behaviour and electrochemical capacitance are further investigated. The assembled all-solid-state symmetrical Cu/RGO/MnO$_{2(6.0)}$ fiber supercapacitor still shows a good fiber shape (Fig. 5a), and a smooth surface is observed in the SEM image due to the uniform coating of the electrolyte gel (Fig. 5b). The obtained fiber supercapacitor also maintains good flexibility, in that it can restore the original straight state after the fiber supercapacitor is bent to 60° for 2 h (Fig. 5c). The electrochemical properties of the flexible all-solid-state symmetrical Cu/RGO/MnO$_{2(6.0)}$ fiber supercapacitor are further characterized by CV and galvanostatic charge–discharge measurements. Although the Cu wire hardly contributes capacitance compared to the Cu/RGO and Cu/RGO/MnO$_{2(6.0)}$ fiber supercapacitors (Fig. S4†), it can be used as a current collector because of its good conductivity. The CV curves of the flexible all-solid-state symmetrical Cu/RGO/MnO$_{2(6.0)}$ fiber supercapacitor remain a quasi-rectangular shape at a scan rate of 50 mV s^{-1} and almost
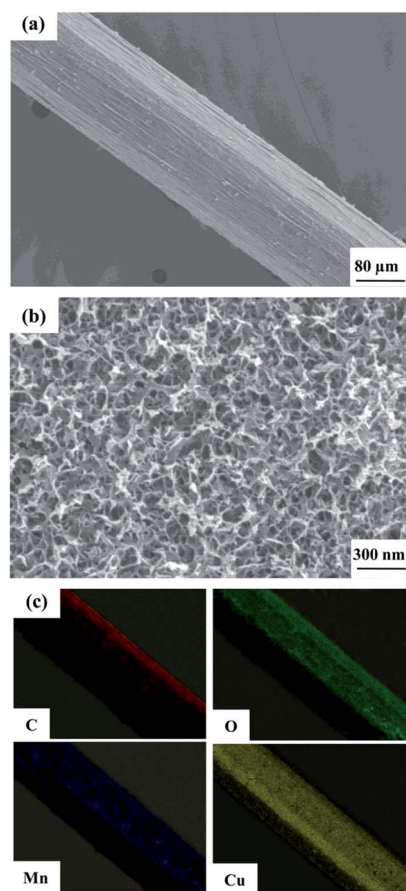

Fig. 3 SEM image (a) with low magnification, FE–SEM image (b) with high magnification, and elemental mapping SEM images (c) of the Cu/RGO/MnO$_{2(6.0)}$ fiber electrode.
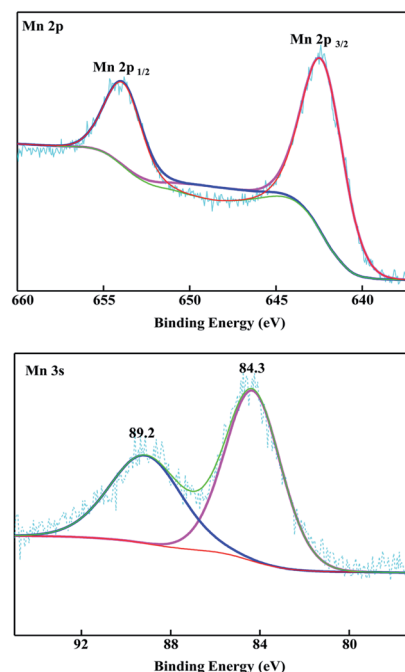

Fig. 4 XPS spectra of the Cu/RGO/MnO$_{2(6.0)}$ fiber electrode: Mn 2p (above) and Mn 3s (below), respectively.
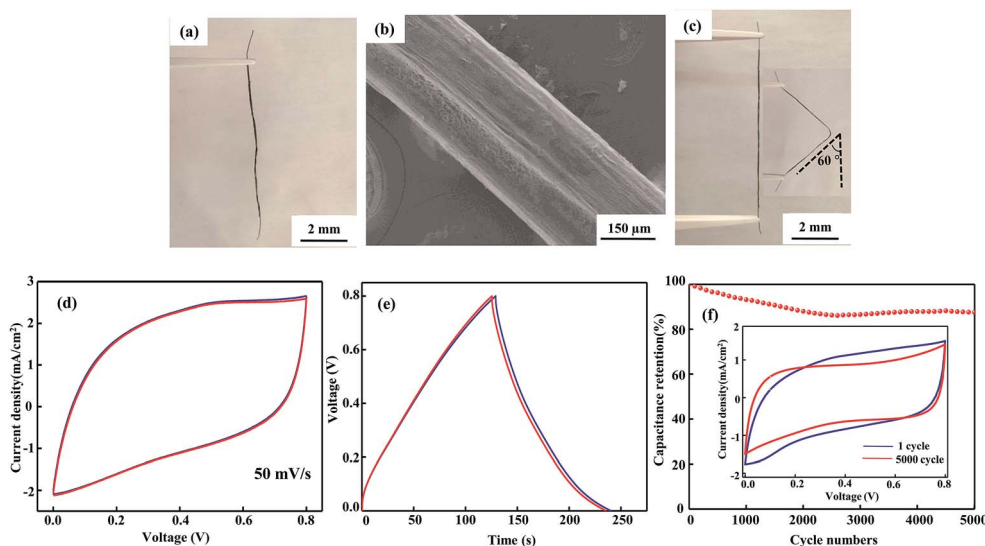
Fig. 5 Photo (a), and SEM image (b), photo of fiber supercapacitor after bending status (c), CV curves (d) and charge–discharge curves (e) at straight and bending status, and the cycle stability at a scan rate of 20 mV s^{-1} after 5000 consecutive cycles (f) of the assembled all-solid-state symmetrical Cu/RGO/MnO$_{2(6.0)}$ fiber supercapacitor.

overlap before and after bending to 60° for 2 h, indicating ideal electrical double-layer capacitance behavior and fast charging–discharging process characteristics (Fig. 5d).[44] Moreover, its galvanostatic charge–discharge curves maintain their typical triangular shape when the flexible all-solid-state symmetrical Cu/RGO/MnO$_{2(6.0)}$ fiber supercapacitor is deformed from the straight to the bending state, further supporting that the assembled all-solid-state symmetrical Cu/RGO/MnO$_{2(6.0)}$ fiber supercapacitor has high flexibility and electrochemical stability (Fig. 5e). In general, when a pseudocapacitive material such as MnO$_2$ or RuO$_2$ is coated on the surface of a RGO fiber, the RGO fiber flexibility is significantly reduced. In the present work, the assembled all-solid-state symmetrical Cu/RGO/MnO$_{2(6.0)}$ fiber supercapacitor still possesses high flexibility although larger amounts of MnO$_2$ are coated on the surface of the Cu/RGO fiber. The good flexibility can be ascribed to two points; one is that the Cu wire as a current collector contributes its flexibility to the Cu/RGO/MnO$_{2(6.0)}$ hybrid fiber, and another is the close contact between MnO$_2$ and the Cu/RGO fiber due to the regular inter-connected MnO$_2$ arrays on the surface of the Cu/RGO fiber. These experimental results also suggest that a suitable coating amount of MnO$_2$ on the surface of the Cu/RGO fiber not only maintains its flexibility, but also improves its capacitance. In addition, the flexible all-solid-state symmetrical Cu/RGO/MnO$_{2(6.0)}$ fiber supercapacitor shows good cycle stability, and 88% of its initial capacitance remains after 5000 consecutive cycles at a scan rate of 20 mV s^{-1} (Fig. 5f). The CV curve after 5000 cycles only shows a relatively slight fluctuation compared with the first cycle, supporting the good stability of the device.

The GCD curves of the flexible all-solid-state symmetrical Cu/RGO/MnO$_{2(6.0)}$ fiber supercapacitor at different current densities ranging from 0.1 to 0.5 mA cm^{-2} are shown in Fig. 6a. The experimental results indicate that the flexible all-solid-state symmetrical Cu/RGO/MnO$_{2(6.0)}$ fiber supercapacitor possesses

good capacitive performance. At a current density of 0.1 mA cm^{-2}, its area specific capacitance is 140 mF cm^{-2} (Table S1†). This value is significantly better than those of a graphene fiber supercapacitor (3.3 mF cm^{-2} at a current density of 0.1 mA cm^{-2})[45] and the flexible all-solid-state graphene/3D porous network-like graphene fiber supercapacitor (1.7 mF cm^{-2} at a current density of 424.6 μA cm^{-2})[46] due to the pseudocapacitive characteristics of MnO$_2$. Also it is much better than those of previously reported RGO/MnO$_2$ hybrid fiber-based supercapacitors, such as a δ-MnO$_2$/holey graphene hybrid fiber supercapacitor (16.7 mF cm^{-2} at a current density of 0.1 mA cm^{-2}),[29] an all-solid-state flexible supercapacitor based on a MnO$_2$/G/GF hybrid fiber (9.6 mF cm^{-2}),[25] the stretchable wire-shaped asymmetric supercapacitors based on pristine and MnO$_2$ coated carbon nanotube fibers (33.75 mF cm^{-2} at a scan rate of 5 mV s^{-1}),[47] and so on (Table S1†). The good area capacitance can be attributed to the synergistic effect associated with the regular inter-connected MnO$_2$ arrays on the surface of the Cu/RGO fiber, the good conductivity of the Cu wire as a current collector, and the close contact between MnO$_2$ and the Cu/RGO fiber. Moreover, in comparison with the area specific capacitance of RGO and the Cu/RGO fiber supercapacitors at various current densities from 0.1 mA cm^{-2} to 0.5 mA cm^{-2}, the area specific capacitance of the Cu/RGO/MnO$_{2(6.0)}$ fiber supercapacitor still remains as high as 68 mF cm^{-2} even at a current density of 0.5 mA cm^{-2}, which is almost four times of RGO and the Cu/RGO fiber supercapacitors (Fig. 6b) due to the pseudocapacitive characteristic of MnO$_2$. Also the area specific capacitance of the Cu/RGO/MnO$_{2(6.0)}$ fiber supercapacitor is barely affected by the mechanical bending, and 97% of its initial capacitance retains after 500 bending cycles with a big angle of 120° (Fig. 6c), suggesting that the all-solid-state symmetrical RGO/MnO$_{2(6.0)}$//RGO/MnO$_{2(6.0)}$ fiber supercapacitor has obvious
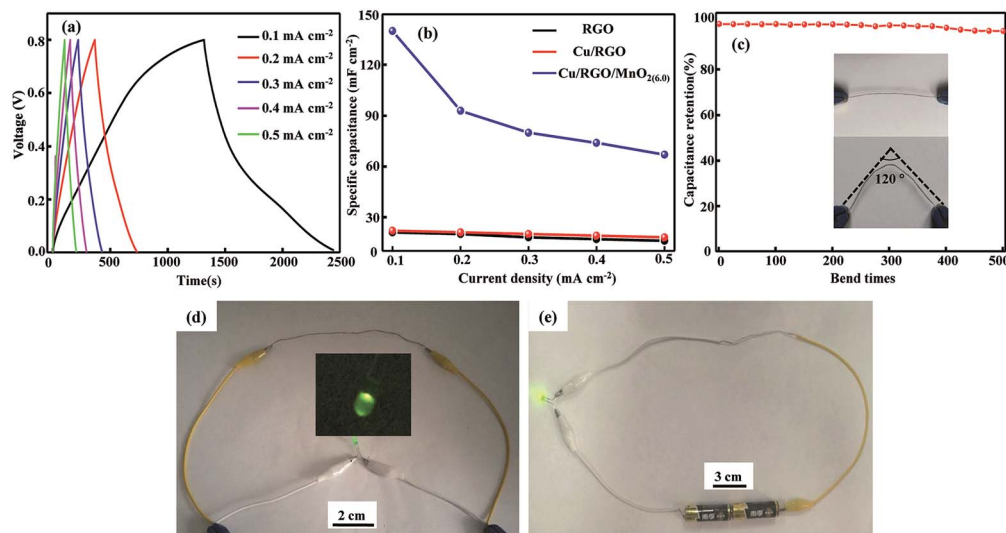
Fig. 6 The specific capacitance at each evaluated current density (a), the capacitance retention at different current densities (b), a relation curve between capacitance retention and bend number (c), lighting up a LED by weaving three fiber-shaped supercapacitors in series (d), and connected with a battery as a electrical cable while the LED is lit (e) of the assembled all-solid-state symmetrical $Cu/RGO/MnO_{2(6.0)}$ fiber supercapacitor.

mechanical property and high area capacitance, good cycling stability and flexibility for practical applications.

By connecting three devices in series, the voltage window of the device can be expanded to 2.4 V from 0.8 V for the single $Cu/RGO/MnO_{2(6.0)}$ fiber supercapacitor with similar discharge time. After being fully charged, the device connected in series can be used to power a light emitting diode (LED) lamp as shown in Fig. 6d, demonstrating its potential application as an efficient energy storage component for flexible electronics. Moreover, a light emitting diode (LED) lamp is also lit (Fig. 6e) when the all-solid-state symmetrical $Cu/RGO/MnO_{2(6.0)}$ fiber supercapacitor is used as an electrical cable and connected to a battery, suggesting that the assembled all-solid-state symmetrical $Cu/RGO/MnO_{2(6.0)}$ fiber supercapacitor can be used as a electrical cable as well as its good energy storage function.

4.   Conclusions

Highly flexible all-solid-state cable-type supercapacitors based on $Cu/RGO/MnO_2$ fibers are successfully assembled by closely placing two $Cu/RGO/MnO_2$ fibers in a parallel orientation and using PVA–KOH gel electrolyte. It can serve as an energy storage device as well as an electrical conduction cable. As an electrode for the energy storage application, the $Cu/RGO/MnO_2$ fibers exhibit excellent enhanced capacitive performance whilst maintaining their flexibility, and a larger area specific capacitance of 140 mF cm^{-2} is obtained at a current density of 0.1 mA cm^{-2} and a 97% capacitance retention is maintained after 500 bending cycles with a big angle of 120°. Aside from its excellent electrochemical performance, it can be used as an electrical cable, and a LED lamp is also lit when it is connected to a battery. These experimental results make the flexible all-solid-state cable-type supercapacitors based on $Cu/RGO/MnO_2$ fibers significantly impactful on future energy storage applications.

Notes and references

1 K. Zhang, H. Hu, W. Yao and C. Ye, *J. Mater. Chem. A*, 2015, **3**, 617–623.
2 H. F. Ju, W. L. Song and L. Z. Fan, *J. Mater. Chem. A*, 2014, **2**, 10895–10903.
3 Z. Niu, W. Zhou, X. Chen, J. Chen and S. Xie, *Adv. Mater.*, 2015, **27**, 6002–6008.
4 X. Xiao, X. Peng, H. Jin, T. Li, C. Zhang, B. Gao, B. Hu, K. Huo and J. Zhou, *Adv. Mater.*, 2013, **25**, 5091–5097.
5 T. Chen and L. Dai, *J. Mater. Chem. A*, 2014, **2**, 10756–10775.
6 S. T. Senthilkumar, Y. Wang and H. Huang, *J. Mater. Chem. A*, 2015, **3**, 20863–20879.
7 L. Dong, C. Xu, Y. Li, Z. H. Huang, F. Kang, Q. H. Yang and X. Zhao, *J. Mater. Chem. A*, 2016, **4**, 4659–4685.
8 Y. Fu, X. Cai, H. Wu, Z. Lv, S. Hou, M. Peng, X. Yu and D. Zou, *Adv. Mater.*, 2012, **24**, 5713–5718.
9 D. Zhang, M. Miao, H. Niu and Z. Wei, *ACS Nano*, 2014, **8**, 4571–4579.
10 W. Ma, S. Chen, S. Yang, W. Chen, W. Weng and M. Zhu, *ACS Appl. Mater. Interfaces*, 2016, **8**, 14622–14627.
11 D. Zhan, J. Yan, L. Lai, Z. Ni, L. Liu and Z. Shen, *Adv. Mater.*, 2012, **24**, 4055–4069.

12 F. Meng, W. Lu, Q. Li, J. H. Byun, Y. Oh and T. W. Chou, *Adv. Mater.*, 2015, **27**, 5113–5131.

13 Y. Hu, H. Cheng, F. Zhao, N. Chen, L. Jiang, Z. Feng and L. Qu, *Nanoscale*, 2014, **6**, 6448–6451.

14 X. Sun, H. Sun, H. Li and H. Peng, *Adv. Mater.*, 2013, **25**, 5153–5176.

15 M. Li, X. Zhang, X. Wang, Y. Ru and J. Qiao, *Nano Lett.*, 2016, **16**, 6511–6515.

16 H. Cheng, C. Hu, Y. Zhao and L. Qu, *NPG Asia Mater.*, 2014, **6**, e113.

17 X. Li, T. Zhao, K. Wang, Y. Yang, J. Wei, F. Kang, D. Wu and H. Zhu, *Langmuir*, 2011, **27**, 12164–12171.

18 J. Bae, M. K. Song, Y. J. Park, J. M. Kim, M. Liu and Z. L. Wang, *Angew. Chem., Int. Ed.*, 2011, **50**, 1683–1687.

19 X. Xiao, T. Li, P. Yang, Y. Gao, H. Jin, W. Ni, W. Zhan, X. Zhang, Y. Cao and J. Zhong, *ACS Nano*, 2012, **6**, 9200–9206.

20 P. Yang, Y. Ding, Z. Lin, Z. Chen, Y. Li, P. Qiang, M. Ebrahimi, W. Mai, C. P. Wong and Z. L. Wang, *Nano Lett.*, 2014, **14**, 731–736.

21 S. W. Lee, S. M. Bak, C. W. Lee, C. Jaye, D. A. Fischer, B. K. Kim, X. Q. Yang, K. W. Nam and K. B. Kim, *J. Phys. Chem. C*, 2014, **118**, 2834–2843.

22 J. Tao, N. Liu, W. Ma, L. Ding, L. Li, J. Su and Y. Gao, *Sci. Rep.*, 2013, **3**, 2286.

23 X. Li, T. Zhao, Q. Chen, P. Li, K. Wang, M. Zhong, J. Wei, D. Wu, B. Wei and H. Zhu, *Phys. Chem. Chem. Phys.*, 2013, **15**, 17752–17757.

24 B. Zheng, T. Huang, L. Kou, X. Zhao, K. Gopalsamy and C. Gao, *J. Mater. Chem. A*, 2014, **2**, 9736–9743.

25 Q. Chen, Y. Meng, C. Hu, Y. Zhao, H. Shao, N. Chen and L. Qu, *J. Power Sources*, 2014, **247**, 32–39.

26 Z. Yu and J. Thomas, *Adv. Mater.*, 2014, **26**, 4279–4285.

27 W. Ma, S. Chen, S. Yang, W. Chen, Y. Cheng, Y. Guo, S. Peng, S. Ramakrishna and M. Zhu, *J. Power Sources*, 2016, **306**, 481–488.

28 Z. Zhang, F. Xiao and S. Wang, *J. Mater. Chem. A*, 2015, **3**, 11215–11223.

29 J. Zhang, X. Yang, Y. He, Y. Bai, L. Kang, H. Xu, F. Shi, Z. Lei and Z. H. Liu, *J. Mater. Chem. A*, 2016, **4**, 9088–9096.

30 Y. Cheng, S. Lu, H. Zhang, C. V. Varanasi and J. Liu, *Nano Lett.*, 2012, **12**, 4206–4211.

31 H. Gao, F. Xiao, C. B. Ching and H. Duan, *ACS Appl. Mater. Interfaces*, 2012, **4**, 2801–2810.

32 Z. Dong, C. Jiang, H. Cheng, Y. Zhao, G. Shi, L. Jiang and L. Qu, *Adv. Mater.*, 2012, **24**, 1856–1861.

33 L. Peng, X. Peng, B. Liu, C. Wu, Y. Xie and G. Yu, *Nano Lett.*, 2013, **13**, 2151–2157.

34 G. Zhang, L. Ren, Z. Yan, L. Kang, Z. Lei, H. Xu, F. Shi and Z. H. Liu, *J. Mater. Chem. A*, 2015, **3**, 14567–14572.

35 Y. Bai, X. Yang, Y. He, J. Zhang, L. Kang, H. Xu, F. Shi, Z. Lei and Z. H. Liu, *Electrochim. Acta*, 2016, **187**, 543–551.

36 C. Julien, *Solid State Ionics*, 2003, **159**, 345–356.

37 L. Zhang, P. Zhu, F. Zhou, W. Zeng, H. Su, G. Li, J. Gao, R. Sun and C. P. Wong, *ACS Nano*, 2016, **10**, 1273–1282.

38 Y. He, Y. Bai, X. Yang, J. Zhang, L. Kang, H. Xu, F. Shi, Z. Lei and Z. H. Liu, *J. Power Sources*, 2016, **317**, 10–18.

39 X. Yang, Y. He, Y. Bai, J. Zhang, L. Kang, H. Xu, F. Shi, Z. Lei and Z. H. Liu, *Electrochim. Acta*, 2016, **188**, 398–405.

40 W. Wei, X. Cui, W. Chen and D. G. Ivey, *Chem. Soc. Rev.*, 2011, **40**, 1697–1721.

41 X. F. Lu, A. L. Wang, H. Xu, X. J. He, Y. X. Tong and G. R. Li, *J. Mater. Chem. A*, 2015, **3**, 16560–16566.

42 M. Toupin, T. Brousse and D. Bélanger, *Chem. Mater.*, 2004, **16**, 3184–3190.

43 P. Ragupathy, D. H. Park, G. Campet, H. N. Vasan, S. J. Hwang, J. H. Choy and N. Munichandraiah, *J. Phys. Chem. C*, 2009, **113**, 6303–6309.

44 W. Liu, N. Liu, Y. Shi, Y. Chen, C. Yang, J. Tao, S. Wang, Y. Wang, J. Su, L. Li and Y. Gao, *J. Mater. Chem. A*, 2015, **3**, 13461–13467.

45 T. Huang, B. Zheng, L. Kou, K. Gopalsamy, Z. Xu, C. Gao, Y. Meng and Z. Wei, *RSC Adv.*, 2013, **3**, 23957–23962.

46 Y. Meng, Y. Zhao, C. Hu, H. Cheng, Y. Hu, Z. Zhang, G. Shi and L. Qu, *Adv. Mater.*, 2013, **25**, 2326–2331.

47 P. Xu, B. Wei, Z. Cao, J. Zheng, K. Gong, F. Li, J. Yu, Q. Li, W. Lu and J. H. Byun, *ACS Nano*, 2015, **9**, 6088–6096.